Author Manuscript

Author Manuscript

Author Manuscript

Author Manuscript

HHS Public Access

Author manuscript

*Gene Ther*. Author manuscript; available in PMC 2016 September 08.

Published in final edited form as:

*Gene Ther*. 2016 June ; 23(6): 520–526. doi:10.1038/gt.2016.24.

# Axonal transport of AAV9 in nonhuman primate brain

**Foad Green**[1], **Lluis Samaranch**[1], **H. Steve Zhang**[2], **Amy Manning-Bog**[2], **Kathleen Meyer**[2], **John Forsayeth**[1], and **Krystof S. Bankiewicz**[1]

[1]Department of Neurological Surgery, University of California San Francisco, San Francisco, 94103 CA

[2]Sangamo Biosciences Inc., Point Richmond Tech Center I, 501 Canal Blvd, Richmond, CA 94804

## Abstract

A pilot study in nonhuman primates (NHP) was conducted in which two Rhesus macaques receive d bilateral parenchymal infusions of adeno-associated virus serotype 9 encoding green fluorescent protein (AAV9-GFP) into each putamen. The post-surgical in-life was restricted to 3 weeks in order to minimize immunotoxicity expected to arise from expression of GFP in antigen-presenting cells. Three main findings emerged from this work. First, the volume over which AAV9 expression was distributed (Ve) was substantially greater than the volume of distribution of MRI signal (Vd). This stands in contrast with Ve/Vd ratio of rAAV2, which is lower under similar conditions. Second, post-mortem analysis revealed expression of GFP in thalamic and cortical neurons as well as dopaminergic neurons projecting from substantia nigra pars compacta, indicating retrograde transport of AAV9. However, fibers in the substantia nigra pars reticulata, a region that receives projections from putamen, also stained for GFP, indicating anterograde transport of AAV9 as well. Finally, one hemisphere received a 10-fold lower dose of vector compared to the contralateral hemisphere ($1.5 \times 10^{13}$ vg/mL) and we observed a much stronger dose-effect on anterograde-linked than on retrograde-linked structures. These data suggest that AAV9 can be axonally transported bi-directionally in primate brain. This has obvious implications to the clinical developing of therapies for neurological disorders like Huntington's or Alzheimer's diseases.

## INTRODUCTION

Axonal transport of AAV is an important aspect of neurological gene therapy, particularly when pressurized infusion techniques, like convection-enhanced delivery (CED), are employed to direct widespread transduction of the primary target domain, e.g. putamen. Co-infusion of an MRI-contrast reagent (chelated gadolinium salt) along with AAV2 into nonhuman primate (NHP) putamen results in an almost perfect overlay of intra-operative MRI contrast with subsequent transgene expression within the primary transduction site.[1, 2]

Users may view, print, copy, and download text and data-mine the content in such documents, for the purposes of academic research, subject always to the full Conditions of use: http://www.nature.com/authors/editorial_policies/license.html#terms

Correspondence should be addressed to: K. S. B. (Krystof.Bankiewicz@ucsf.edu), Department of Neurosurgery, University of California San Francisco, 1855 Folsom Street, MCB, Room 226, San Francisco, CA 94103. Tel: (415) 502-3132; Fax: (415) 514-2864.

No competing financial interests exist.

Author Manuscript Author Manuscript Author Manuscript Author Manuscript

The correlation breaks down somewhat when one considers the phenomenon of axonal transport of AAV, since the contrast reagent reflects only distribution within the primary infusion site.

We have shown previously that AAV2 is a neurotropic vector that is transported in an anterograde direction along neurons when it is infused into the parenchyma of rat and NHP brain.[3, 4] This transport of intact viral particles is sufficiently robust that vector is apparently released from projecting nerve terminals where it is able to transduce distal post-synaptic neurons. Thus, infusion of AAV2 into NHP thalamus resulted in robust transduction of cortical neurons contained entirely within the cortex. In contrast, AAV6 is transported along axons in a retrograde direction and is almost as neurotropic as is AAV2.[5, 6] For example, transduction of NHP putamen results in transgene expression in cortico-striatal neurons. These observations motivated us to ask whether other serotypes also show directionality in axonal transport. We extended our investigation of this phenomenon to AAV9, because it is being actively explored for neurological gene therapy applications.

In this study, 2 NHP received infusions of AAV9-GFP bilaterally into putamen. AAV9 differed strikingly from AAV2 and AAV6 in terms of axonal transport and cell-type specificity. AAV9 transduced astrocytes and neurons but not microglia. The vector was transported axonally in both anterograde and retrograde directions. These data advance our understanding of AAV9 distribution in the primate brain and provides support for its use in the treatment of neurological disease with a substantial cortico-striatal pathology such as Huntington's disease.

## RESULTS

### Infusion and transduction efficiency

In this study, 2 NHP received putaminal infusions of AAV9-GFP at either a high dose (HD; left hemisphere; $1.5 \times 10^{13}$ vg/mL) or a low dose (LD; right hemisphere; $1.5 \times 10^{12}$ vg/mL). The post-surgical in-life phase was intentionally kept short (3 weeks) in order to limit potential confounds arising from cell-mediated responses to GFP as previously described.[7, 8] The distribution of gadolinium signal was evaluated volumetrically by infusate 3D modeling of MRI as previously described.[9] Reconstruction of Gad signal revealed that coverage of the putamen infusate was almost complete (Fig. 1). In addition, GFP expression was superimposable onto a reconstruction of putamen from the baseline sequence of MR images at various coronal levels. The overlap between GFP and gadolinium signal indicated that the infusate was well-contained in the target structure with little leakage into the anterior and medial portions of the putamen. Also, analysis showed that GFP distribution in the target side was three times larger than the Gad signal (Fig. S1). This is quite different from what we have seen with AAV2 where expression of transgene correlated almost exactly with the MRI signal.[1]

Immunohistochemical analysis of tissue sections from the injection site showed robust transgene expression both in left (HD) and right (LD) putamina with an abundance of cell bodies and neuronal fibers (Fig. 2a). No neuronal loss was found after AAV9-GFP infusion regardless of the dose (Fig. 2b). To analyze neuronal transduction by AAV9-GFP, GFP+/

Author Manuscript Author Manuscript Author Manuscript Author Manuscript

NeuN+ cells were counted in serial sections from the injection site in two different locations as previously described.[7] Cell counting was performed within the highly transduced area, i.e. the primary area of transduction (PAT), and outside the primary area of transduction (oPAT), 350 μm away from PAT, where GFP-positive neuronal expression diminished sharply. Interestingly, GFP+/NeuN+ cell counting showed identical levels of expression in both PAT and oPAT regardless of the administered dose, comparing one hemisphere to another (Fig. 2c). These results are consistent with our previous observations of a relatively slow build-up of anti-GFP responses, not evident at 3 weeks,[7, 8] although we saw evidence of activation of microglia and MHC-II upregulation (Fig. S2).

There are a number of mechanisms for antigen-presentation in the brain, mainly astrocytes[10] and microglia.[11] To determine the cellular specificity of AAV9, we immunostained brain sections for the transgene and cell-specific markers, including marker for neurons (NeuN), for astrocytes (GFAP) and a microglia (Iba1) at the infusion site (Fig. S3). Double immunofluorescence staining against GFP with each of the cellular markers revealed transgene was readily expressed in both neurons and astrocytes, whereas microglia were not transduced despite massive GFP expression in neighboring cell bodies and neuronal fibers. Nevertheless, activation of microglia in transduced regions was easily observable (Fig. S2), indicative of the ability of microglia to sense the innate immune status of their local environment.

## Axonal transport

Infusion of AAV9-GFP into putamen yielded transduction in distal structures. GFP staining was observed, for example, in cell bodies of the prefrontal, frontal, and parietal cortex (Fig. 3). GFP-positive cell bodies and fibers were also present in thalamus, globus pallidus and components of the basal ganglia, including the substantia nigra pars compacta (SNc) and pars reticulata (SNr), as well as subthalamic nucleus (STN) and in fibers of the medial forebrain bundle (MFB) (Fig. 4). There was a strong dose-dependence of axonal transport to distal loci. Thus, a high but not low dose of AAV9 resulted in cell body labeling in STN despite the fact that there is no direct neuronal connection between the putamen and STN. We have previously noted such indirect anterograde transport within basal ganglia with AAV2[3, 4] and from thalamus to cortex.[12] However, the significant dose-dependence of AAV9-GFP transport implies a 2-stage transport of vector first to the globus pallidus and then to STN. This anterograde transport of AAV9 was further indicated by the presence of GFP-positive fibers and cell bodies within the SNr (Fig. 4S). Surprisingly, retrograde transport from putamen to SNc was also confirmed by the presence of GFP-positive cell bodies in SNc, a structure that projects to putamen (Fig. 5S). In addition, although not as dramatic as in STN, there was a clear dose effect of AAV9-GFP on transduction in these areas. Thus, we conclude that AAV9 is transported along axons in both directions, a phenomenon that accounts at least partly for the remarkable distribution of AAV9 in the primate brain.

Author Manuscript Author Manuscript Author Manuscript Author Manuscript

## DISCUSSION

As clinical development of neurological gene therapy with vectors based on adeno-associated virus (AAV) becomes more common, the behavior of specific serotypes of AAV in the primate brain is becoming more important. This is particularly true in the context of more advanced vector infusion technologies that are driving clinical development of neurosurgical interventions in diseases such as Parkinson's disease[2] and rare neurological disorders such as aromatic L-amino acid decarboxylase (AADC) deficiency.[13] This new technique employs intra-operative MRI to visualize parenchymal infusions of AAV2. Its utility is derived from the remarkable correlation between distribution of MRI contrast reagent and eventual transgene expression. With AAV2, the ultimate volume of transgene expression (Ve) and the intra-operative volume of distribution (Vd) are identical.[1] However, this close correlation breaks down somewhat with AAV9. AAV9 Ve was significantly greater than Vd (~3-fold), emphasizing the important role of interstitial or perivascular transport processes engaged as result of the initial pressurized infusion (CED).[14] In the case of AAV2, we would argue that the avidity of the vector for abundant heparan sulphate proteoglycans[15] helps to restrict AAV2 to the infusion site and matches Ve closely with Vd. In contrast, the primary receptor for AAV9 is not HSPG[16] and this vector may thus engage the perivasculature to achieve a much greater Ve for a given infusion volume (Vi).

AAV9 evinces a broad tropism in neural tissues,[17–19] transducing neurons and astrocytes as well as perhaps other cell types. The ability of AAV9 to transduce antigen-presenting cells (APC) in the brain has risen concerns with respect to expression of foreign (non-self) proteins[7, 8, 20] in APC and the consequent engagement of neurotoxic adaptive immune responses. This, of course, is not likely to be a problem when self-proteins are expressed, but in the present study we observed, as previously, activation of Iba1 and upregulation of MHC-II on astrocytes and microglia (Fig. S2). Both types of glia are brain APC that have unique individual functions. However, we saw no evidence of microglial transduction by AAV9-GFP, even though these cells were clearly responsive to GFP presentation. Our conclusion is that astrocytes are the key APC with respect to adaptive responses to GFP expression.

One of the most striking discoveries about the behavior of AAV serotypes in the brain has been the phenomenon of axonal transport. Although the ability of viruses to be transported over long distances thought neuronal projections was initially described in Herpes simplex[21–24] and Rabies virus,[25–28] the transport of intact AAV particles over long distances have been described also in AAV2. [29] In contrast to the primarily retrograde transport of the above viruses, in our hands AAV2 undergoes anterograde transport in CNS neurons;[3, 4, 12] that is, particles of AAV2 are transported intact from neuronal cell bodies to synaptic terminals where they are released to be taken up by neurons in distal locations. This phenomenon requires very efficient distribution and transduction at the primary transduction location and it may explain why it was not discovered earlier since only CED can really achieve this degree of efficiency. Infusion of AAV2 into NHP thalamus results in widespread cortical expression of transgene, primarily in pyramidal neurons located in cortical lamina V/VI. Similarly, transduction of NHP putamen or rat striatum with AAV2 results in transgene expression in cell bodies within SNr, which receives projections from striatal

Author Manuscript Author Manuscript Author Manuscript Author Manuscript

GABAergic neurons, but not SNc, which projects to striatum. In contrast to the anterograde transport of AAV2, AAV6 is transported in an exclusively retrograde direction and is almost as neurotropic as AAV2.[5, 6] Accordingly, we have started to examine this phenomenon in other AAV serotypes.

Axonal transport of AAV9 was found in this study to be bi-directional. Infusion of AAV9-GFP into putamen lead to transgene expression in cortico-striatal neurons that project to putamen and GFP expression was also found in SNc neurons, thereby confirming retrograde transport of this serotype (Fig. 5S). This phenomenon, significantly more efficient than seen with AAV6,[6] is potentially very valuable in devising therapies for Huntington's disease in which degeneration of both basal ganglionic and cortico-striatal neurons is central to the neuropathology of the disease.[30] Efficient transduction of human putamen with a therapeutic AAV9 would correct the massive degeneration of the striatal medium spiny neurons and, would potentially enable cortical projections and transduce the extensive area that is the cortex. In addition, viral transport could also benefit the treatment of other affected distal areas like thalamus, hippocampus and white matter. The axonal transport, in conjunction with the long-term expression, is in fact, the central advantages of this technology to find a future treatment for Huntington diseases in contrast to other explored non-viral options like the administration of trophic factors or siRNA.

Additionally, however, vector was transported in an anterograde direction to SNr and to STN (Fig. 5). Labeling of STN neurons was highly dependent on vector dose (Fig. 4), more so than in SNr, suggesting a dose requirement for transport of AAV9-GFP via an indirect route through globus pallidus (GP). It is unclear at the present whether transport of vector from putamen to GP proceeds by axonal or perivascular transport. In rats, we found evidence for rapid movement of AAV2 and fluorescent liposomes into GP from striatum and ascribed this rapid movement to perivascular pumping.[14] This phenomenon has not been directly explored in the primate brain, however, although the ability of AAV9 to spread efficiently beyond the initial putaminal infusion volume (Fig. S1) suggests a powerful perivascular mechanism. Nevertheless, the phenomenon of bidirectional axonal transport of AAV9 may explain in part why this vector is regarded with such enthusiasm for applications in which very widespread distribution of vector is essential. It does, however, suggest that untoward transport might bring with it some drawbacks and these will need to be elucidated in the context of specific gene therapies.

## MATERIALS AND METHODS

### Animals

Two rhesus monkeys (*Macaca mulatta*, 4–15 years of age, >4kg) were included in this study. Experiments were performed according to National Institutes of Health guidelines and to protocols approved by the Institutional Animal Care and Use Committee at University of California San Francisco.

Author Manuscript Author Manuscript Author Manuscript Author Manuscript

### Vector preparation

AAV9-containing green fluorescent protein (GFP) under the control of the cytomegalovirus promoter was generated by triple transfection of HEK-293 cells as previously described.[31] AAV9-GFP generated was supplied by ReGenX Inc (Washington, D. C.) and was diluted immediately before use to a concentration of $1.4 \times 10^{13}$ vg/ml (high dose) or $1.4 \times 10^{12}$ vg/ml (low dose) in phosphate-buffered saline and 0.001% (vol/vol) Pluronic F-68.

### Surgery and vector infusion

Each NHP underwent stereotactic placement of skull-mounted, MR-compatible temporary plastic plugs. The animal was then placed supine in an MRI-compatible stereotactic frame. After craniectomy, the cannula-guides were secured to the skull over both hemispheres. After placement of the plugs, the intubated animal was moved to the platform table in the MRI suite and placed on inhaled isoflurane (1–3%). Guides under sterile conditions were filled with MR-visible tracer (Prohance, Singem, Germany) to localize the plugs in the MR images to calculate the trajectory to the target structures inside the brain. Then, the NHP was moved into the MR magnet and high-resolution anatomical MR scan was acquired for target identification and surgical planning. After the target was selected, a custom-designed, ceramic, fused silica reflux-resistant cannula with a 3-mm stepped tip was used for vector infusion as described previously.[2, 32, 33] The cannula was attached to a 1-ml syringe mounted onto an MRI-compatible infusion pump (Harvard Apparatus, Boston, MA). The infusion initiated at 1μl/min, and after visualizing the infusate at the cannula tip, the cannula was introduced through the guide-stem into the brain. When the depth-stop encountered the top of the guide-stem, it was secured with a locking screw. The infusion rate was ramped up from an initial 1 μl/min to a final 5 μl/min. Each NHP received infusions covering the pre- and post-commissural putamen simultaneously in each putamen (bilateral). The total infusion volume per hemisphere was 100 μl in both hemispheres. Once the infusion ended, guide-devices were removed from the skull, and animals were returned to their home cages and monitored during recovery from anesthesia.

### MRI acquisition

Animals were scanned on a Siemens Verio Magnetom 3.0T MRI (Siemens, Malvern, PA). T1-weighted fast low angle shot (FLASH) acquisitions obtained with a 4° flip angle on the first scan produced a proton-density weighted image to trace gadolinium at the cannula tip (8 ms TE, 28 ms TR, 3 excitations, 256 × 3 × 192 matrix, 14 × 14 mm field of view, 1 mm slices). All subsequent scans were serially acquired at a 40° flip angle to increase the T1-weighting and highlight the Gd signal enhancement.

### Tissue processing

Animals infused with AAV9 were perfused transcardially approximately 3 weeks after AAV-GFP infusion with cold saline followed by 4% paraformaldehyde. Brains were harvested and histologically analyzed using previously established methods. In short, 6mm coronal blocks were collected via a brain matrix and immediately post-fixed in paraformaldehyde overnight, then cryoprotected in 30% (w/v) sucrose the following day. A sliding microtome was used to

Author Manuscript Author Manuscript Author Manuscript Author Manuscript

cut 40-um serial sections. Chromogenic staining was performed on free-floating sections to visualize GFP expression by methods we have previously established.

## Immunohistochemistry

For each serotype, sections were collected in sequence, stored in cryoprotectant solution (0.5 M sodium phosphate buffer, pH 7.4, 30% glycerol, and 30% ethylene glycol) at 4°C until further processing. Immunohistochemistry was performed on free-floating sections. Briefly, washes with PBS for the horseradish peroxidase (HRP)-based procedure, or in PBS with 0.1% Tween 20 (PBST) for fluorescence staining, were performed between each immunohistochemical step. Endogenous peroxidase activity (for peroxidase-based procedures) was quenched for 30 min at room temperature (RT). Blocking of non-specific staining was accomplished by incubation of sections in 20% horse serum in PBST for 60 min at RT. Thereafter, sections were incubated overnight with specific primary antibodies as follows: polyclonal rabbit anti-Iba1, PAb, 1:500 (www.biocare.net/); monoclonal mouse and anti-GFAP, 1:10,000 for HRP-based staining and polyclonal rabbit and anti-GFAP 1:1000 for fluorescence (www.millipore.com); monoclonal mouse anti-NeuN, 1:5,000 for HRP-based staining and 1:500 for fluorescence staining (www.millipore.com); monoclonal and mouse anti-TH, 1:1000 (www.millipore.com, MAB318); polyclonal mouse and monoclonal rabbit anti-GFP, 1:200 and 1:500, respectively, (www.lifetechnologies.com, Cat. G10362; www.millipore.com, MAB3580). All antibodies were dissolved in Da Vinci diluent (www.biocare.net/). After 3 rinses in PBS for 5 min at RT, sections for HRP-based staining were incubated with either Mach 2 anti-mouse HRP polymer (www.biocare.net/) or March 2 anti-rabbit HRP polymer (www.biocare.net/) for 1 h at RT. The activity of bound HRP was visualized by means of a commercially available kit with 3,3′-diaminobenzidine peroxide substrate (www.vectorlabs.com/). NeuN-stained sections were counterstained with Cresyl Violet stain. Finally immunostained sections were mounted on gelatinized slides, dehydrated in alcohol and xylene and cover-slipped with Cytoseal (www.fishersci.com/).

For dual fluorescent immunostaining of different antigens (GFP/GFAP, GFP/NeuN, GFP/TH, and GFP/Iba1), a combination of primary antibodies was applied to sections as a cocktail of primary antibodies by overnight incubation at 4°C. All primary antibodies were dissolved in Da Vinci diluent (www.biocare.net/). After three washes in PBST, monoclonal primary antibodies were visualized by incubation in the dark for 2 h with appropriate secondary fluorochrome-conjugated antibodies: goat anti-mouse DyLight 549 (red) (www.biocare.net/), goat anti-rabbit DyLight 549, donkey anti-rabbit Alexa Fluor 555 (www.lifetechnologies.com/), goat anti-mouse DyLight 488 (green), goat anti-rabbit DyLight 488, and donkey anti-rabbit Alexa Fluor 488. All secondary antibodies were dissolved at 1:1,000 dilution in Fluorescence Antibody Diluent (www.biocare.net/). Sections were cover-slipped with Vectashield Hard Set, mounting medium for fluorescence (www.vectorlabs.com/). Control sections were processed without primary antibodies, and no significant immunostaining was observed under these conditions.

## Semi-quantitative Analyses

Distribution volume (Vd) was determined with Brainlab iPlan Flow Suite (Brainlab, Munich, Germany; www.brainlab.com). Infusion sites, cannula tracts and cannula tip were

Author Manuscript Author Manuscript Author Manuscript Author Manuscript

identified on T1-weighted MR images in the coronal, axial, and sagittal planes. Regions of interest (ROI) were delineated to outline T1 gadolinium signal and target putamen. Three-dimensional volumetric reconstructions of the image series and ROI were analyzed to estimate Vd of infusions and ratio to Vi.

### Analysis of brain sections

All sections were examined and digitally photographed on a Zeiss Axioskop microscope (www.zeiss.com/) equipped with CCD color video camera and image analysis system (Axiovision Software; www.zeiss.com/). For each monkey, the number of GFP-positive and NeuN-positive cells was determined in both hemispheres from coronal sections through the putamen. Fluorescence microscopy was used to determine the number of double-labeled cells in sections. Photomicrographs for double-labeled sections were obtained by merging images from two separate channels (red-rhodamine and green-fluorescein isothiocyanate; co-localization appears yellow) without altering the position of the sections or focus (objective x 20 and x 40, Carl Zeiss microscopy with ApoTome mode). For each double staining, sections were selected anterior and posterior ~500 μm from the site of injection. To estimate the proportion of cells expressing GFP/NeuN, GFP/GFAP, GFP/TH and GFP/Iba1, each section was analyzed by first using one channel for the presence of phenotype-specific cells (TH, GFAP, Iba1, or NeuN) and a second combined channel for the number of co-stained cells.

Sections stained for NeuN and GFP were used for counting from three sections at three different levels of the injection site in the putamen (bilateral). NeuN positive and GFP positive cells were counted at 200-fold magnification from 5 randomly acquired frames (350 $\mu m^2$) in both the transduced area. In the non-transduced area, 5 randomized frames were taken 350 μm from the defined border of expression. These analyses permitted semi-quantitative comparisons, although they do not reflect the total number of transduced cells *in vivo*. Cell counts in each sampled region were averaged across sections for each animal and the final data are presented as the mean number of NeuN-positive and GFP-positive cells.

## Supplementary Material

Refer to Web version on PubMed Central for supplementary material.

## Acknowledgments

This study was funded by Sangamo Inc. (Point Richmond, CA) and by an NIH-NINDS grant to KSB (R01NS073940-01).

## References

1. Fiandaca MS, Varenika V, Eberling J, McKnight T, Bringas J, Pivirotto P, et al. Real-time MR imaging of adeno-associated viral vector delivery to the primate brain. Neuroimage. 2009; 47(Suppl 2):T27–35. [PubMed: 19095069]
2. Richardson RM, Kells AP, Rosenbluth KH, Salegio EA, Fiandaca MS, Larson PS, et al. Interventional MRI-guided putaminal delivery of AAV2-GDNF for a planned clinical trial in Parkinson's disease. Mol Ther. 2011; 19:1048–1057. [PubMed: 21343917]

Author Manuscript Author Manuscript Author Manuscript Author Manuscript


3. Ciesielska A, Mittermeyer G, Hadaczek P, Kells AP, Forsayeth J, Bankiewicz KS. Anterograde axonal transport of AAV2–GDNF in rat basal ganglia. Mol Ther. 2011; 19:922–927. [PubMed: 21102559]
4. Kells AP, Forsayeth J, Bankiewicz KS. Glial-derived neurotrophic factor gene transfer for Parkinson's disease: anterograde distribution of AAV2 vectors in the primate brain. Neurobiol Dis. 2012; 48:228–235. [PubMed: 22019719]
5. Salegio EA, Samaranch L, Kells AP, Mittermeyer G, San Sebastian W, Zhou S, et al. Axonal transport of adeno-associated viral vectors is serotype-dependent. Gene Ther. 2012
6. San Sebastian W, Samaranch L, Heller G, Kells AP, Bringas J, Pivirotto P, et al. Adeno-associated virus type 6 is retrogradely transported in the non-human primate brain. Gene Ther. 2013; 20:1178–1183. [PubMed: 24067867]
7. Ciesielska A, Hadaczek P, Mittermeyer G, Zhou S, Wright JF, Bankiewicz KS, et al. Cerebral infusion of AAV9 vector-encoding non-self proteins can elicit cell-mediated immune responses. Mol Ther. 2013; 21:158–166. [PubMed: 22929660]
8. Samaranch L, San Sebastian W, Kells AP, Salegio EA, Heller G, Bringas JR, et al. AAV9-mediated expression of a non-self protein in nonhuman primate central nervous system triggers widespread neuroinflammation driven by antigen-presenting cell transduction. Mol Ther. 2014; 22:329–337. [PubMed: 24419081]
9. Richardson RM, Kells AP, Martin AJ, Larson PS, Starr PA, Piferi PG, et al. Novel platform for MRI-guided convection-enhanced delivery of therapeutics: preclinical validation in nonhuman primate brain. Stereotact Funct Neurosurg. 2011; 89:141–151. [PubMed: 21494065]
10. Cornet A, Bettelli E, Oukka M, Cambouris C, Avellana-Adalid V, Kosmatopoulos K, et al. Role of astrocytes in antigen presentation and naive T-cell activation. J Neuroimmunol. 2000; 106:69–77. [PubMed: 10814784]
11. Nelson PT, Soma LA, Lavi E. Microglia in diseases of the central nervous system. Ann Med. 2002; 34:491–500. [PubMed: 12553488]
12. Kells AP, Hadaczek P, Yin D, Bringas J, Varenika V, Forsayeth J, et al. Efficient gene therapy-based method for the delivery of therapeutics to primate cortex. Proc Natl Acad Sci U S A. 2009; 106:2407–2411. [PubMed: 19193857]
13. San Sebastian W, Kells AP, Bringas J, Samaranch L, Hadaczek P, Ciesielska A, et al. SAFETY AND TOLERABILITY OF MRI-GUIDED INFUSION OF AAV2-hAADC INTO THE MID-BRAIN OF NON-HUMAN PRIMATE. Mol Ther Methods Clin Dev. 2014; 3
14. Hadaczek P, Yamashita Y, Mirek H, Tamas L, Bohn MC, Noble C, et al. The "perivascular pump" driven by arterial pulsation is a powerful mechanism for the distribution of therapeutic molecules within the brain. Mol Ther. 2006; 14:69–78. [PubMed: 16650807]
15. Summerford C, Samulski RJ. Membrane-associated heparan sulfate proteoglycan is a receptor for adeno-associated virus type 2 virions. J Virol. 1998; 72:1438–1445. [PubMed: 9445046]
16. Shen S, Bryant KD, Brown SM, Randell SH, Asokan A. Terminal N-linked galactose is the primary receptor for adeno-associated virus 9. J Biol Chem. 2011; 286:13532–13540. [PubMed: 21330365]
17. Gray SJ, Matagne V, Bachaboina L, Yadav S, Ojeda SR, Samulski RJ. Preclinical Differences of Intravascular AAV9 Delivery to Neurons and Glia: A Comparative Study of Adult Mice and Nonhuman Primates. Mol Ther. 2011; 19:1058–1069. [PubMed: 21487395]
18. Hinderer C, Bell P, Vite CH, Louboutin J-P, Grant R, Bote E, et al. Widespread gene transfer in the central nervous system of cynomolgus macaques following delivery of AAV9 into the cisterna magna. Molecular Therapy — Methods & Clinical Development. 2014; 1
19. Foust KD, Nurre E, Montgomery CL, Hernandez A, Chan CM, Kaspar BK. Intravascular AAV9 preferentially targets neonatal neurons and adult astrocytes. Nat Biotechnol. 2009; 27:59–65. [PubMed: 19098898]
20. Forsayeth J, Bankiewicz KS. Transduction of antigen-presenting cells in the brain by AAV9 warrants caution in preclinical studies. Mol Ther. 2015; 23:612. [PubMed: 25849423]
21. Costantini LC, Jacoby DR, Wang S, Fraefel C, Breakefield XO, Isacson O. Gene transfer to the nigrostriatal system by hybrid herpes simplex virus/adeno-associated virus amplicon vectors. Hum Gene Ther. 1999; 10:2481–2494. [PubMed: 10543613]

Author Manuscript Author Manuscript Author Manuscript Author Manuscript

22. Diefenbach RJ, Miranda-Saksena M, Douglas MW, Cunningham AL. Transport and egress of herpes simplex virus in neurons. Rev Med Virol. 2008; 18:35–51. [PubMed: 17992661]
23. Lilley CE, Groutsi F, Han Z, Palmer JA, Anderson PN, Latchman DS, et al. Multiple immediate-early gene-deficient herpes simplex virus vectors allowing efficient gene delivery to neurons in culture and widespread gene delivery to the central nervous system in vivo. J Virol. 2001; 75:4343–4356. [PubMed: 11287583]
24. McGraw HM, Friedman HM. Herpes simplex virus type 1 glycoprotein E mediates retrograde spread from epithelial cells to neurites. J Virol. 2009; 83:4791–4799. [PubMed: 19279108]
25. Gillet JP, Derer P, Tsiang H. Axonal transport of rabies virus in the central nervous system of the rat. J Neuropathol Exp Neurol. 1986; 45:619–634. [PubMed: 2430067]
26. Kelly RM, Strick PL. Rabies as a transneuronal tracer of circuits in the central nervous system. J Neurosci Methods. 2000; 103:63–71. [PubMed: 11074096]
27. Klingen Y, Conzelmann KK, Finke S. Double-labeled rabies virus: live tracking of enveloped virus transport. J Virol. 2008; 82:237–245. [PubMed: 17928343]
28. Larsen DD, Wickersham IR, Callaway EM. Retrograde tracing with recombinant rabies virus reveals correlations between projection targets and dendritic architecture in layer 5 of mouse barrel cortex. Front Neural Circuits. 2007; 1:5. [PubMed: 18946547]
29. Kaspar BK, Llado J, Sherkat N, Rothstein JD, Gage FH. Retrograde viral delivery of IGF-1 prolongs survival in a mouse ALS model. Science. 2003; 301:839–842. [PubMed: 12907804]
30. Berardelli A, Noth J, Thompson PD, Bollen EL, Curra A, Deuschl G, et al. Pathophysiology of chorea and bradykinesia in Huntington's disease. Mov Disord. 1999; 14:398–403. [PubMed: 10348461]
31. Matsushita T, Elliger S, Elliger C, Podsakoff G, Villarreal L, Kurtzman GJ, et al. Adeno-associated virus vectors can be efficiently produced without helper virus. Gene Ther. 1998; 5:938–945. [PubMed: 9813665]
32. Krauze MT, Saito R, Noble C, Tamas M, Bringas J, Park JW, et al. Reflux-free cannula for convection-enhanced high-speed delivery of therapeutic agents. J Neurosurg. 2005; 103:923–929. [PubMed: 16304999]
33. Fiandaca MS, Forsayeth JR, Dickinson PJ, Bankiewicz KS. Image-guided convection-enhanced delivery platform in the treatment of neurological diseases. Neurotherapeutics. 2008; 5:123–127. [PubMed: 18164491]

Author Manuscript Author Manuscript Author Manuscript Author Manuscript

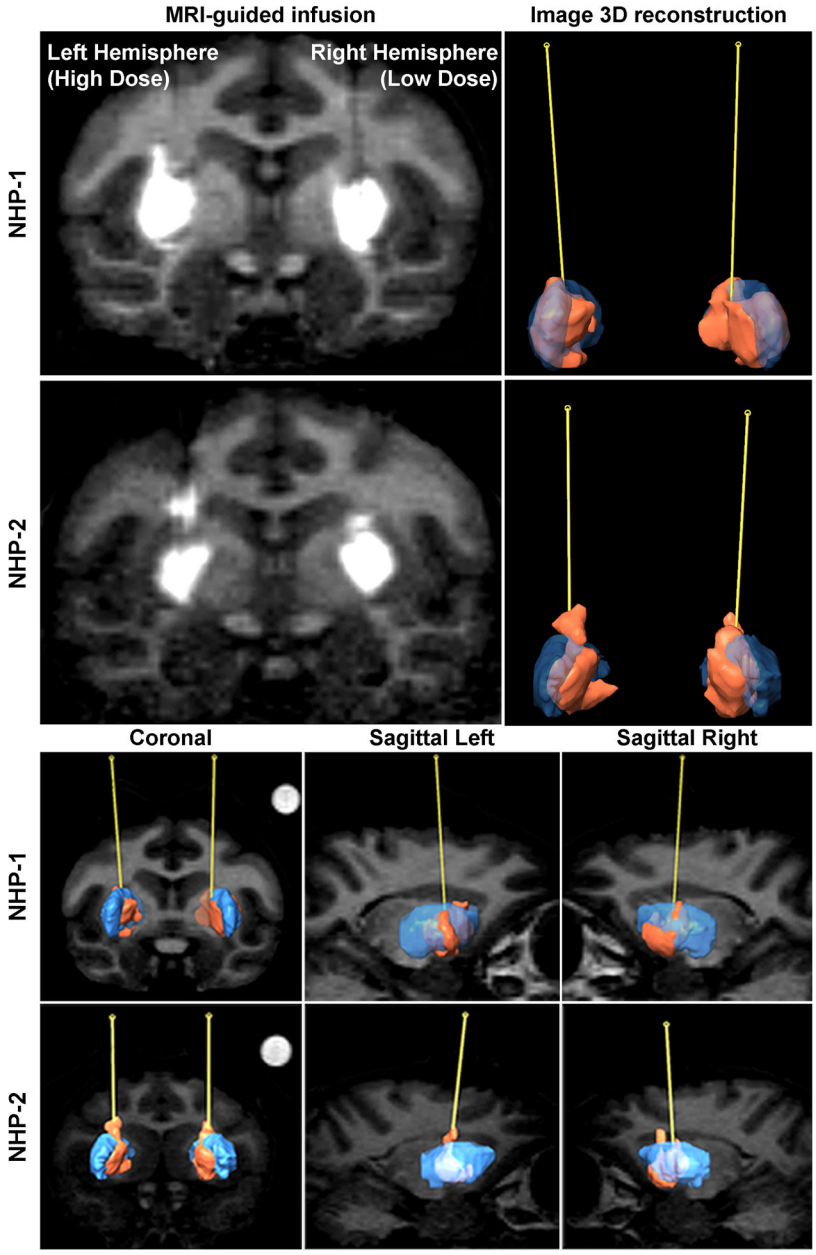


**Figure 1. Evaluation of the infusion**

A comparative panel is shown for the MRI-guided infusion of AAV9-GFP (100 μL) into the bilateral putamen of normal nonhuman primates (NHP; n=2; *top* and *bottom*). Reconstructed volume for each putamen (n=4), labeled in blue, measured approximately 850 μL for NHP-1 and 625 μL for NHP-2. The infusate containing AAV9-GFP particles and chelated gadolinium imaging reagent, labeled in orange, distributed into approximately 350 μL for each infusion. The coronal and sagittal (left and right) planes offer comparative views of the cannula trajectory paths between animals.

Author Manuscript Author Manuscript Author Manuscript Author Manuscript

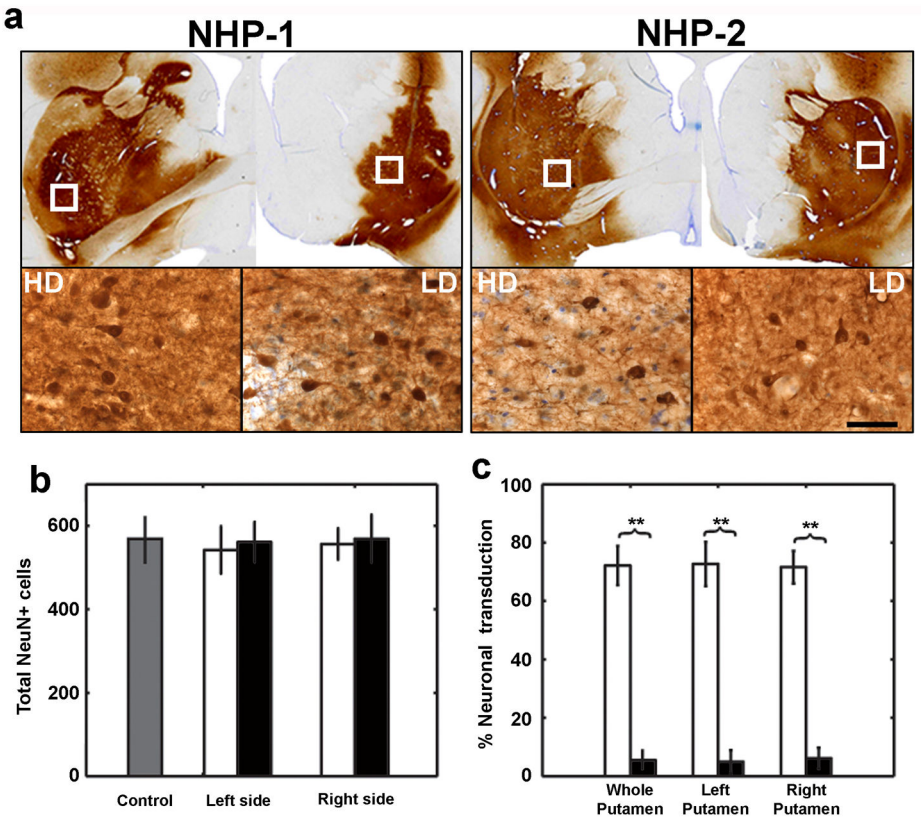


**Figure 2. AAV9-mediated GFP expression in the putamen**

Representative section of brain tissue showed robust GFP staining within the putamen at the infusion site **(a, top)**. High-magnification images (*white squares*) depict GFP-positive cells in putamen administered either a high dose (left hemisphere, $1.5 \times 10^{13}$ vg/mL) or low dose (right hemisphere, $1.5 \times 10^{12}$ vg/mL) of vector **(a, bottom)**. NeuN-positive cells counted within the putamen in three consecutive coronal sections showed no significant difference ($p>0.05$) both in high- (*black bar*) and low-dosed hemispheres (*white bar*) compared with naïve NHP control (*grey bar*) **(b)**. Transduced neurons ($GFP^+/NeuN^+$) were counted within the putamen in 3 consecutive coronal sections at PAT (*white bar*) and oPAT (*black bar*), showed about 74% transduction efficiency in PAT and 5% in oPAT ($p<0.01$). Data are expressed as mean ± SD. Wilcoxon sign-ranked *S*-test. Scale bars: 50 μm.

Author Manuscript Author Manuscript Author Manuscript Author Manuscript

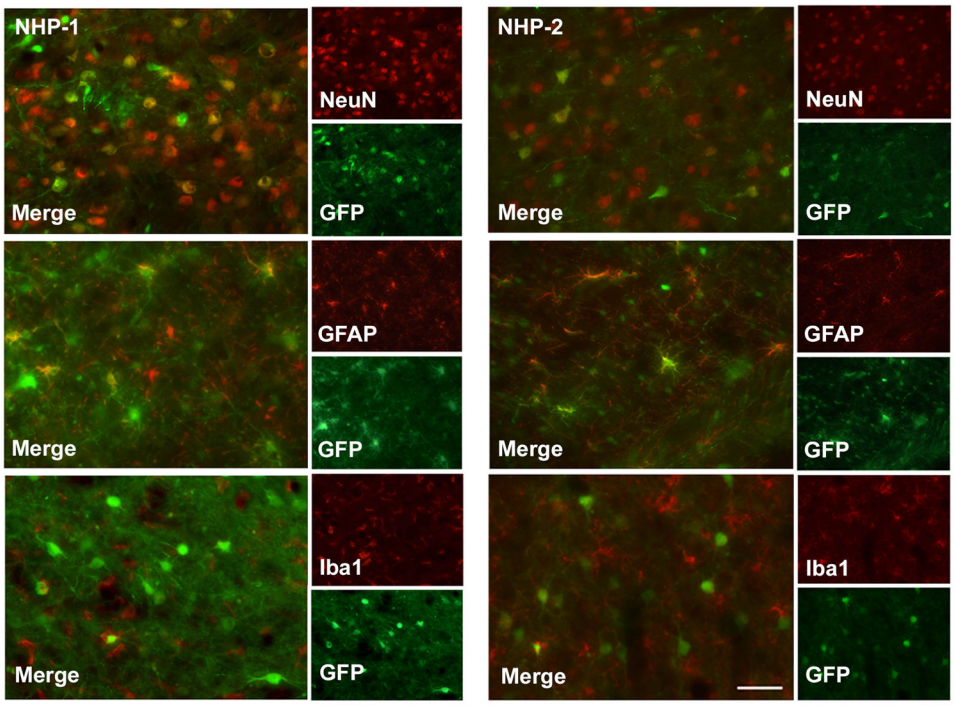


**Figure 3. Axonal transport thought cortico-striatal pathway**

Immunostaining against GFP revealed neuron-like transduced cells in cortex on the anterio-posterior axis after putaminal infusion (top), suggesting retrograde axonal transport of AAV9 from putamen to cortex. High-dose hemisphere revealed stronger transduction levels in cortical cell bodies and fibers (**i** and **iii**) compared with low-dose hemisphere (**ii** and **iv**) in both animals, indicating a strong dose effect. Scale bars: 200 μm.

Author Manuscript Author Manuscript Author Manuscript Author Manuscript

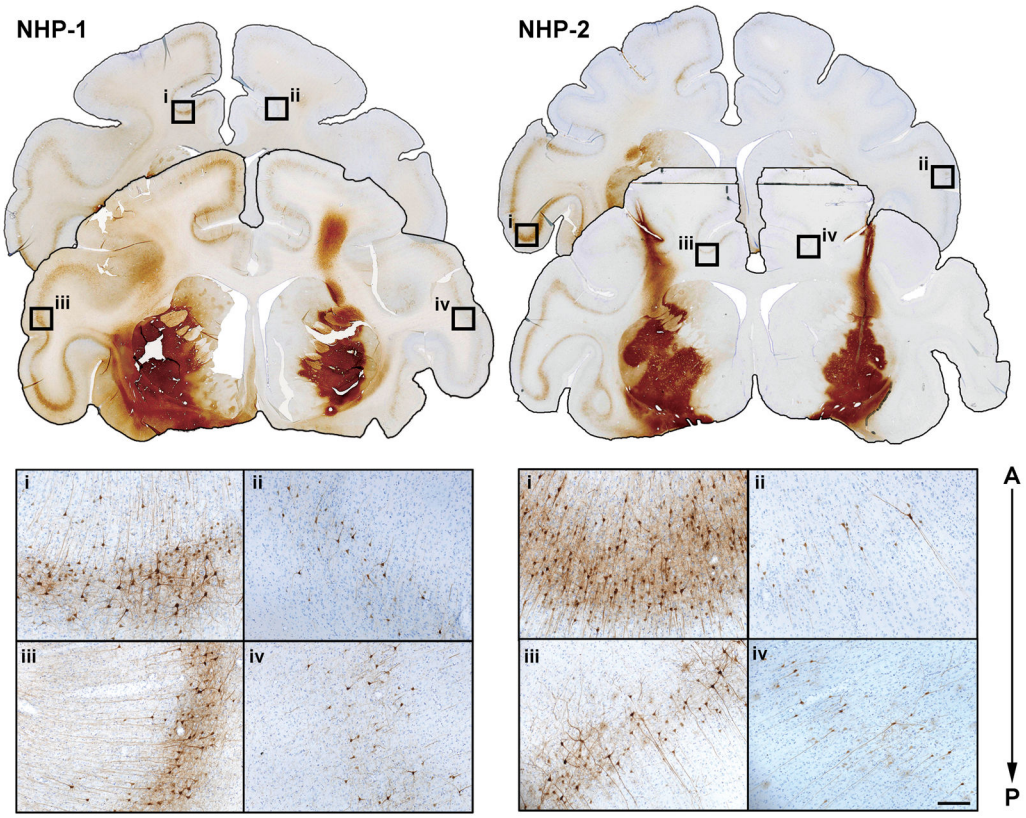


**Figure 4. Axonal transport to distal regions**

Infusion of AAV9 into the putamen resulted in GFP-positive cells in many distal regions known to receive projections from the putamen, suggesting also an anterograde transport. Shown is anti-GFP immunohistochemistry with approximate position of each coronal section 12 mm posterior to the cannula tract. High-magnification images correspond to the left and right hemispheres of the globus pallidus (GP), thalamus, subthalamic nucleus (STN), medial forebrain bundle (MFB), and substantia nigra (SN). Scale bars: 500μm.